Ullah et al., http://www.jgp.org/cgi/content/full/jgp.201110753/DC1

1 Supplemental Material

1.1 IP_3R Obeys Detailed Balance

To show that the ligand binding kinetics of IP_3Rs are consistent with the thermodynamics principle of detailed balance, we follow the procedure in (Song and Magleby, 1994). We obtain two-dimensional dwell time distributions of adjacent open and closed times in the forward direction from the time-series data from IP_3R under three different Ca^{2+} (100 nM, 1 μM, and 89 μM) and fixed IP_3 (10 μM) concentrations. We use the logs of the open duration and the following closed duration to locate a bin on the x-y plane. We use 5 bins per log unit. We repeat the same procedure by logarithmically binning the pairs of adjacent open and closed intervals in the backward (reverse) direction on the time-series data. A reversible gating mechanism gives similar results for forward and backward analysis of the data. Forward and backward two-dimensional distributions based on over 280000 events (where an event is an open-closed pair) are shown in Fig. S1. As in (Song and Magleby, 1994), we use the χ^2 test for the significant differences between the two distributions. A χ^2 value is calculated from

$$\chi^2 = \sum_{i,j} \frac{[F(i,j) - E(i,j)]^2}{E(i,j)} + \frac{[B(i,j) - E(i,j)]^2}{E(i,j)}. \quad (1)$$

Where $F(i,j)$ and $B(i,j)$ refer to the number of events in bin (i,j) for the forward and backward distributions, respectively, and $E(i,j) = [F(i,j)+B(i,j)]/2$ is the average number of events in bin (i,j) for both the forward and backward distributions. The summation in eq. 1 is restricted to those bins with five or more events in both the forward and backward distributions, and the degrees of freedom, D, is given by the total number of such pairs (Song and Magleby, 1994). Finally, we calculate the approximate normal deviate $Z = \sqrt{(2\chi^2)} - \sqrt{(2D-1)}$ to estimate significance. Observed differences are significant at the 5% level if $Z > 1.96$ (Snedecor and Cochran, 1989). We get $Z = -1.82$ from our analysis. Thus, our data are consistent with the microscopic reversibility hypothesis.

1.2 The Equilibrium Occupancies Contain No Information Regarding Network Connectivity

In general a finite state Markov chain obeys an evolution equation $dp/dt = pQ$ where p is a vector with $p_\ell(t)$ being the probability that the ℓ^{th} state is occupied at time t given an initial

probability vector at $t = 0$. Q is the "generator matrix": $Q_{\mathrm{ij}}, \mathrm{i} \neq \mathrm{j}$ is the transition rate from state i to state j. The diagonal entries are given by $Q_{\mathrm{ii}} = -\sum_{\mathrm{j}\neq\mathrm{i}} Q_{\mathrm{ij}}$ which is an expression of conservation of probability (Bruno et al., 2005). The last equality has an immediate consequence: if u is the vector containing all ones, $Qu = 0$. We assume, given Q, that there is a unique stationary solution, w, such that $wQ = 0$ with normalization $w \cdot u = 1$. The uniqueness assumption implies that there is a finite time path between every pair of states. If the static solution is a state of thermodynamic equilibrium then every reaction must be in detailed balance: $w_{\mathrm{i}}Q_{\mathrm{ij}} = w_{\mathrm{j}}Q_{\mathrm{ji}}$. As shown above, the IP_3R gating kinetics obey detailed balance. We define a diagonal matrix W with $W_{\mathrm{ii}} = w_{\mathrm{i}}$. The detailed balance condition is: $WQ = (WQ)^{\mathrm{T}}$ where T indicates the matrix transpose. We define the flux matrix $Q^{\mathrm{flux}} = WQ$. Q^{flux} is a symmetric generator matrix. Its off-diagonal entries, $Q^{\mathrm{flux}}_{\mathrm{ij}}, \mathrm{i} \neq \mathrm{j}$ give the flux from state i to state j at equilibrium. Since Q^{flux} is a generator, $Q^{\mathrm{flux}}u = 0$. Since Q^{flux} is symmetric, it follows that $u^{\mathrm{T}}Q^{\mathrm{flux}} = 0$ as well. Note that the equilibrium occupancies are encoded within W while the network connectivity is encoded within Q^{flux}. It follows that equilibrium occupancy data such as P_{o} contain no information about the network connectivity. This is because the equilibrium occupancy vector w contains no information about network connectivity. To see this, note that $wQ = wW^{-1}Q^{\mathrm{flux}} = u^{\mathrm{T}}Q^{\mathrm{flux}} = 0$ so that given a Q^{flux}, any conformant w is a stationary vector of Q. Note that Q is similar to a symmetric matrix $\hat{Q} = W^{1/2}QW^{-1/2} = W^{-1/2}Q^{flux}W^{-1/2}$.

1.3 Do missed events cause more error in P_{o} or in τ_{o} or τ_{c}?

We claim that error in τ_{o} and τ_{c} due to missed events is greater than the error in P_{o}. We have not found a rigorous proof for this statement but we expect it because although error in τ_{o} and τ_{c} result in error in P_{o} some of the error cancels. Indeed, if τ_{o} and τ_{c} have the same error which might be very large, there is no resulting error in the P_{o}. We provide some analysis in support of our claim. Initially we assume that the time series is meaningfully described as binary but make no assumptions with regard to the gating. That is, the channel can be declared as either "open" or "closed" at every point in time; there are no sub-conductance levels etc.

We introduce the following quantities: T, the length of time the experiment ran, N, the true number of open events (which is equal to the number of closed events) that occurred, F, the fraction of events that were observed ($0 \leq F \leq 1$), the "true" mean open and closed times: τ_{o}, τ_{c}, and the true equilibrium open probability: P_{o}, along with the observed open and closed time, and open probability: τ_{o}^{obs}, τ_{c}^{obs}, P_{o}^{obs}. (By "true" mean open and closed times

we mean the true sample average which we assume is representative of the actual average.) Note that since these errors are from *missed* events we necessarily have that $\tau_{\rm o}^{obs} > \tau_{\rm o}$ and $\tau_{\rm c}^{obs} > \tau_{\rm c}$. If the true number of openings and closings is N then the true mean open and closed times obey:

$$N(\tau_{\rm o} + \tau_{\rm c}) = T \ . \tag{2}$$

If only FN, of events are observed then observed mean open and closed times, $\tau_{\rm o}^{obs}$ and $\tau_{\rm c}^{obs}$, obey:

$$FN(\tau_{\rm o}^{obs} + \tau_{\rm c}^{obs}) = T \tag{3}$$

from which it follows that

$$(\tau_{\rm o}^{obs} + \tau_{\rm c}^{obs}) = \frac{1}{F}(\tau_{\rm o} + \tau_{\rm c}) \ . \tag{4}$$

The observed and actual open probabilities obey:

$$P_{\rm o} = \frac{\tau_{\rm o}}{\tau_{\rm o} + \tau_{\rm c}} \tag{5}$$

$$P_{\rm o}^{obs} = \frac{\tau_{\rm o}^{obs}}{\tau_{\rm o}^{obs} + \tau_{\rm c}^{obs}} \ . \tag{6}$$

We define the fractional error in $\tau_{\rm o}$, $\tau_{\rm c}$, $P_{\rm o}$, as $\Delta_{\rm o}$, $\Delta_{\rm c}$, and Δ_P respectively.

$$\Delta_{\rm o} \equiv 1 - \frac{\tau_{\rm o}}{\tau_{\rm o}^{obs}} \geq 0 \tag{7}$$

$$\Delta_{\rm c} \equiv 1 - \frac{\tau_{\rm c}}{\tau_{\rm c}^{obs}} \geq 0 \tag{8}$$

$$\Delta_P \equiv 1 - \min\left(\frac{P_{\rm o}}{P_{\rm o}^{obs}}, \frac{P_{\rm o}^{obs}}{P_{\rm o}}\right) \geq 0 \tag{9}$$

These definitions place all fractional errors in the unit interval. Combining Eqs(4-8) we have

$$F = \frac{\tau_{\rm o} + \tau_{\rm c}}{\tau_{\rm o}^{obs} + \tau_{\rm c}^{obs}} = \frac{(1-\Delta_{\rm o})(1-\Delta_{\rm c})}{P_{\rm c}(1-\Delta_{\rm o}) + P_{\rm o}(1-\Delta_{\rm c})} \tag{10}$$

where $P_{\rm c} = 1 - P_{\rm o}$ and

$$P_{\rm o}^{obs} = \frac{\tau_{\rm o}^{obs}}{\tau_{\rm o}^{obs} + \tau_{\rm c}^{obs}} = \frac{\frac{\tau_{\rm o}}{1-\Delta_{\rm o}}}{\frac{\tau_{\rm o}}{1-\Delta_{\rm o}} + \frac{\tau_{\rm c}}{1-\Delta_{\rm c}}} = \frac{F}{1-\Delta_{\rm o}} P_{\rm o} \ . \tag{11}$$

Note that if $\Delta_{\rm o} > \Delta_{\rm c}$ then $P_{\rm o}^{obs} > P_{\rm o}$. If $\Delta_{\rm c} > \Delta_{\rm o}$ then $P_{\rm o} > P_{\rm o}^{obs}$. Along the line $\Delta_{\rm o} = \Delta_{\rm c}$ we have $P_{\rm o} = P_{\rm o}^{obs}$ so that $\Delta_P = 0$ (the red dotted line in Fig. S2). In the figure

we have plotted the curves $\Delta_P = \Delta_o$ (solid lines, black: $P_o = 0.9$, blue: $P_o = 0.01$) which is given by

$$\Delta_c = \frac{\Delta_o \left(P_c + 1 - \Delta_o + \Delta_o P_o\right)}{P_c + \Delta_o P_o} \tag{12}$$

and $\Delta_P = \Delta_c$ (dashed lines, black: $P_o = 0.9$, blue: $P_o = 0.01$) which is given by:

$$\Delta_c = 1 - \frac{1}{2}P_o - \sqrt{P_c - \Delta_o + \Delta_o P_o + {P_o}^2} \ . \tag{13}$$

Note that it is always the case that $\Delta_P \leq \max(\Delta_o, \Delta_c)$. Between the dashed and solid blue lines it is also true that $\Delta_P \leq \min(\Delta_c, \Delta_o)$ for $P_o = 0.01$. Similarly, between the dashed and solid black lines it is also true that $\Delta_P \leq \min(\Delta_c, \Delta_o)$ for $P_o = 0.9$. We have treated Δ_o and Δ_c as independent and thus our results hold for any (Δ_o, Δ_c) pair. In general though, Δ_o and Δ_c are not independent; missed openings result in longer closed times and missed closings result in longer open times. This fact tends to push the system closer to the line $\Delta_o = \Delta_c$ where $\Delta_P = 0$.

1.4 Occupancy and Flux

To illustrate the concept of occupancy and flux parameters and their relation with reaction rates, we consider the following sequence involving three states in which the channel sequentially binds two molecules of ligand L:

$$\mathrm{A} + \mathrm{L} \underset{k_{\mathrm{TA}}}{\overset{k_{\mathrm{AT}}}{\rightleftharpoons}} \mathrm{T} \tag{14}$$

$$\mathrm{T} + \mathrm{L} \underset{k_{\mathrm{BT}}}{\overset{k_{\mathrm{TB}}}{\rightleftharpoons}} \mathrm{B} \tag{15}$$

where k_{AT}, k_{TA}, k_{TB}, and k_{BT} denote the reaction rate constants. We pick the unliganded state (or complex) A as the reference state and give it unit unnormalized occupancy, $Z_{\mathrm{A}} = 1$. Unnormalized occupancies of other states in this reaction sequence, T and B, are the equilibrium probabilities of the channel being in these states relative to the probability of it being in state A. This relation carries over into the more complex Markov chain we must deal with in modeling the IP_3R channel. The combined laws of mass action and detailed balance imply that the unnormalized occupancy of every state is proportional to L^n, where $L = [\mathrm{L}]$, and n is the number of ligand molecules bound to that state. We call the proportionality constant the occupancy parameter of that state. For the reaction sequence in (14) and (15), the unnormalized equilibrium occupancy for T is $Z_{\mathrm{T}} = K_{\mathrm{T}} L$,

where $K_{\rm T} \equiv k_{\rm AT}/k_{\rm TA}$ is the occupancy parameter of state T; the unnormalized occupancy of B is $Z_{\rm B} = K_{\rm B}L^2$ and $K_{\rm B} \equiv K_{\rm T}(k_{\rm TB}/k_{\rm BT})$ is the occupancy parameter of state B. Thus, the occupancy parameter of a state is the product of all forward equilibrium constants for the reactions connecting the reference state to that state through an arbitrary path. The *normalized* occupancies of A, T, and B is then $\pi_{\rm A} = 1/Z$, $\pi_{\rm T} = Z_{\rm T}/Z$, and $\pi_{\rm B} = Z_{\rm B}/Z$, respectively, with $Z = 1+K_{\rm T}L+K_{\rm B}L^2$. Throughout the main text and SI text, Z represents the total unnormalized occupancy of all states involved in a reaction sequence, $Z^{\rm M}$ that of all states in a gating mode M, $Z_{\rm o}$ that of the "open aggregate" consisting of all open complexes, $Z_{\rm c}$ that of the "closed" aggregate consisting of all closed complexes, and $Z_{\rm o}^{\rm M}$ that of all open complexes in mode M.

The unnormalized flux between states T and B, $J_{\rm TB}$, is the product of $Z_{\rm T}$ and the reaction rate from T to B, $r_{\rm TB}$. So $r_{\rm TB} = J_{\rm TB}/Z_{\rm T}$. Since T and B are in equilibrium, $J_{\rm TB} = J_{\rm BT}$ and $r_{\rm BT} = J_{\rm TB}/Z_{\rm B}$. The flux parameter $j_{\rm AT}$ for the A + L $\rightleftharpoons$ T reaction is defined as the proportionality constant for the flux from A to T in terms of L. The flux from A to T: $J_{\rm AT} = r_{\rm AT}Z_{\rm A} = k_{\rm AT}L = j_{\rm AT}L$. Similarly, $J_{\rm TB} = k_{\rm TB}LZ_{\rm T} = k_{\rm TB}K_{\rm T}L^2 = j_{\rm TB}L^2$, where $j_{\rm TB}$ is the flux parameter for the T + L $\rightleftharpoons$ B reaction. Since the flux from A to T must balance that from T to A: $k_{\rm TA}Z_{\rm T} = k_{\rm TA}K_{\rm T}L = j_{\rm AT}L$; and flux from T to B balances that from B to T: $k_{\rm BT}Z_{\rm B} = k_{\rm BT}K_{\rm B}L^2 = j_{\rm TB}L^2$. Thus, the four rate constants can be expressed in terms of flux parameters $j_{\rm AT}$ and $j_{\rm TB}$, and occupancy parameters $K_{\rm T}$ and $K_{\rm B}$: $k_{\rm AT} = j_{\rm AT}$, $k_{\rm TB} = j_{\rm TB}/K_{\rm T}$, $k_{\rm TA} = j_{\rm AT}/K_{\rm T}$, and $k_{\rm BT} = j_{\rm TB}/K_{\rm B}$.

1.5 Low-occupancy States

We consider the reaction sequence in Eqs(14–15) to explain the concept of low-occupancy states and model simplification procedure. If $K_{\rm T} = 0.1\ \mu{\rm M}^{-1}$ and $(k_{\rm TB}/k_{\rm BT}) = 100\ \mu{\rm M}^{-1}$, $K_{\rm B} = K_{\rm T}(k_{\rm TB}/k_{\rm BT}) = 10\ \mu{\rm M}^{-2}$. Then $Z_{\rm T}$ is maximum when $L = K_{\rm B}^{-1/2}$, at which point $Z_{\rm A}$ and $Z_{\rm B} = 1$ and $Z_{\rm T} \approx 0.03$ only. The relative high rates from T to A and B results in such low occupancy for T that it is not detectable in $P_{\rm o}$ data. State T is therefore a transition state and the reaction chain can be simplified to an *effective chain* A $\rightleftharpoons$ B with renormalized rates. Since each forward reaction in the full chain involves ligand binding, the backward reaction in the effective chain is ligand dependent. The effective flux between A and B, $J_{\rm AB}^{\rm eff}$ is given by (see also SI section 1.6):

$$\frac{1}{J_{\rm AB}^{\rm eff}} = \left(\frac{1}{J_{\rm AT}} + \frac{1}{J_{\rm TB}}\right) = \left(\frac{1}{j_{\rm AT}L} + \frac{1}{j_{\rm TB}L^2}\right)\ . \tag{16}$$

The effective rate from A to B = $J^{\rm eff}_{\rm AB}/Z_{\rm A} = J^{\rm eff}_{\rm AB} = j_{\rm AT}\ j_{\rm TB}L^2/(j_{\rm AT} + j_{\rm TB}L)$ and the effective rate from B to A = $J^{\rm eff}_{\rm AB}/Z_{\rm B} = J^{\rm eff}_{\rm AB}/K_{\rm B}L^2 = j_{\rm AT}\ j_{\rm TB}/(j_{\rm AT} + j_{\rm TB}L)K_{\rm B}$, where $K_{\rm B}$ is the occupancy parameter for B. The simplified approximating reaction sequence can thus be characterized by two flux parameters ($j_{\rm AT}$ and $j_{\rm TB}$) and one occupancy parameter ($K_{\rm B}$) instead of four parameters. Note that both effective rates from A to B and from B to A are L dependent.

Proper treatment of low-occupancy states is crucial, both for getting the rates right in the simplified model and for obtaining a model structure with learnable parameters. Without the simplification, the search to optimize the fit to data with the reaction chain will be conducted in a 4-dimensional parameter space when there are effectively only 3 parameters. Keeping the transition state T will result in a neutral direction (a direction in which all fits are equally good) in the space of parameters.

Although the transition state T has very low occupancy, it nevertheless plays a key role serving as a "speed bump" to reduce the effective flux between A and B as L increases. For small L, $J^{\rm eff}_{\rm AB} \approx j_{\rm TB}L^2$ while for large L, $J^{\rm eff}_{\rm AB} \approx j_{\rm AT}L$.

The effective chain A $\rightleftharpoons$ B will yield more rapid transitions than the true chain. In the full chain, there are two reactions going from state A to state B so there cannot be any instantaneous transition from A to B when L is abruptly changed from 0 to some finite level. So the distribution of latencies (*i.e.* first passage times) from A to B is zero at $t = 0$. The distribution of latencies for the approximating chain is a single decaying exponential: $J^{\rm eff}_{\rm AB}\ exp(-J^{\rm eff}_{\rm AB}t)$, and therefore nonzero at $t = 0$. However, the probability of making the transition from A to B by time t for the exact and approximating chains converges even for small (non-zero) t.

Applying such simplifications by excluding transition states can result in substantial reduction in the number of parameters required to specify more complex systems.

1.6 Model Simplification

We simplify various branches in the model that have low-occupancy transition states as described in the previous section. For example, in the chain $\rm C^I_{04} \rightleftharpoons T_{14} \rightleftharpoons C^H_{24}$, $\rm T_{14}$ is a transition state with 1 $\rm Ca^{2+}$ and 4 $\rm IP_3$ bound. The only states that we are including in the model have 0 and 4 $\rm Ca^{2+}$ bound. Clearly there is a "missing state" ($\rm T_{14}$ in this example) which mediates the transition between state $\rm C^I_{04}$, which has no $\rm Ca^{2+}$ bound, and state $\rm C^H_{24}$, which has two $\rm Ca^{2+}$ bound. The $P_{\rm o}$ data are not adequate to provide accurate estimates of the occupancy of the transition states save that their occupancy is always low relative to

that of the primary states in the model. Note that this does not imply that the occupancy of T_{14} is less than the occupancy of C_{00} for all Ca^{2+} concentration. Rather, it means that the occupancy of T_{14} is negligible compared to at least one of the main states in any conditions. Applying Occam's razor, we set the occupancy of all the required low-occupancy transition states to zero. As we pointed out above, these states don't disappear entirely, they serve as "speed bumps" for the probability flux between high occupancy states.

Using the analogy between flux and conductance in an electrical circuit, the transition rates between various states can be derived as follows. The effective conductance of a linear chain of resistors is the reciprocal of the sum of the reciprocal conductances of the individual resistors. Thus it will prove useful to define a function for the reciprocal of a sum of reciprocals, rsr:

$$rsr(x_1, x_2, \cdots\ x_n) \equiv \frac{1}{\sum_{i=1}^{n} \frac{1}{x_i}}\ . \tag{17}$$

Note that $rsr(\alpha x_1, \alpha x_2, \cdots\ \alpha x_n) = \alpha\ rsr(x_1, x_2, \cdots\ x_n)$, a property that we will make frequent use of. The effective flux for the transition $C_{04}^{I} \rightleftharpoons C_{24}^{H}$ is given by

$$J^{\text{eff}}_{C_{04}^{I} C_{24}^{H}} = rsr(J_{C_{04}^{I} T_{14}}, J_{T_{14} C_{24}^{H}}) \tag{18}$$

where $J_{X_{\lambda\mu} Y_{\nu\rho}}$ represents the flux from state $X_{\lambda\mu}$ (with λ Ca^{2+} and μ IP_3 bound) to state $Y_{\nu\rho}$ (with ν Ca^{2+} and ρ IP_3 bound). This is analogous to replacing a circuit with two resistors connected in series with the equivalent single-resistor circuit. The flux between $X_{\lambda\mu}$ and $Y_{\nu\rho}$ is proportional to $\mathcal{C}^{\zeta}\mathcal{I}^{\eta}$ where ζ is the maximum of λ and ν, and η is the maximum of μ and ρ (Yang et al., 2006). The proportionality constant is the *flux parameter*: $j_{\lambda\mu\nu\rho}$. Thus $J_{C_{04}^{I} T_{14}} = j_{0414}\mathcal{C}\mathcal{I}^4$ and $J_{T14 C_{24}^{H}} = j_{1424}\mathcal{C}^2\mathcal{I}^4$. We can rewrite Eq. 18 as

$$J^{\text{eff}}_{C_{04}^{I} C_{24}^{H}} = \mathcal{C}\mathcal{I}^4\ rsr(j_{0414}, j_{1424}\mathcal{C}) \tag{19}$$

The flux from one state to another is simply the product of the occupancy of the initial state and the rate from initial to final state, i.e.

$$J^{\text{eff}}_{C_{04}^{I} C_{24}^{H}} = \text{Occupancy of } C_{04}^{I} \times \text{Rate from } C_{04}^{I} \text{ to } C_{24}^{H}\ . \tag{20}$$

The occupancy of C_{04}^{I} is $K_{C_{04}^{I}}\mathcal{I}^4$, therefore

$$\text{Rate from } C_{04}^{I} \text{ to } C_{24}^{H} = \frac{\mathcal{C}}{K_{C_{04}^{I}}} rsr\left(j_{0414}, j_{1424}\mathcal{C}\right)\ . \tag{21}$$

Since the fluxes we are parameterizing are equilibrium fluxes, $J^{\text{eff}}_{\text{C}^{\text{H}}_{24}\text{C}^{\text{I}}_{04}} = J^{\text{eff}}_{\text{C}^{\text{I}}_{04}\text{C}^{\text{H}}_{24}}$. With the occupancy of state $\text{C}^{\text{H}}_{24} = K_{\text{C}^{\text{H}}_{24}}\mathcal{C}^2\mathcal{I}^4$, we have

$$\text{Rate from } \text{C}^{\text{H}}_{24} \text{ to } \text{C}^{\text{I}}_{04} = \frac{1}{K_{\text{C}^{\text{H}}_{24}}\mathcal{C}} rsr\left(j_{0414}, j_{1424}\mathcal{C}\right) \ . \tag{22}$$

Note that for small $\mathcal{C}$, the rate from C^{I}_{04} to $\text{C}^{\text{H}}_{24} \approx j_{1424}\mathcal{C}^2/K_{\text{C}^{\text{I}}_{04}}$. For large $\mathcal{C}$, rate from C^{I}_{04} to $\text{C}^{\text{H}}_{24} \approx j_{0414}\mathcal{C}/K_{\text{C}^{\text{I}}_{04}}$. The rest of the rates between various states are derived using the above analogy and are tabulated in Table S2.

Although 4 transitions are required to go from C^{L}_{00} to C^{I}_{04}, we parameterized the effective flux, $J^{\text{eff}}_{\text{C}^{\text{L}}_{00}\text{C}^{\text{I}}_{04}}$, with only two parameters:

$$J^{\text{eff}}_{\text{C}^{\text{L}}_{00}\text{C}^{\text{I}}_{04}} = rsr(j_{0001}\mathcal{I}, j_{0102}\mathcal{I}^2, j_{0203}\mathcal{I}^3, j_{0304}\mathcal{I}^4) = rsr(j_{0001}\mathcal{I}, j_{0304}\mathcal{I}^4) \tag{23}$$

by assuming that the fluxes between the 01 and 02 and between the 02 and 03 transition states to be infinite so that they are not rate limiting. This is done because we only have sufficient data to define two flux parameters. Similarly, only one flux parameter each can be defined from the data for the $\text{C}^{\text{L}}_{30} \rightleftharpoons \text{C}^{\text{L}}_{32}$ and $\text{C}^{\text{L}}_{32} \rightleftharpoons \text{C}^{\text{L}}_{34}$ transitions.

To minimize the number of parameters, we assume that the effective rates for the reactions $\text{C}^{\text{I}}_{04} \rightarrow \text{C}^{\text{I}}_{24}$, $\text{C}^{\text{L}}_{00} \rightarrow \text{C}^{\text{L}}_{20}$ and $\text{C}^{\text{I}}_{04} \rightarrow \text{C}^{\text{H}}_{24}$ **are the same**. Similarly, the effective rates for the reactions $\text{C}^{\text{I}}_{04} \leftarrow \text{C}^{\text{I}}_{24}$, $\text{C}^{\text{L}}_{00} \leftarrow \text{C}^{\text{L}}_{20}$ and $\text{C}^{\text{I}}_{04} \leftarrow \text{C}^{\text{H}}_{24}$ **are the same** (see Table S2).

Flux parameters used to calculate the transition rates are given in Table S3 and are estimated as follows. Ligand dependencies of some of the transition rates are shown in Fig. S3.

1.7 Estimation of Flux Parameters

For the initial guess, we constrain the flux parameters according to the mean latencies, modal mean open times, and modal lifetimes (Mak et al., 2007; Ionescu et al., 2007). For example, to calculate the flux parameter for $\text{C}^{\text{H}}_{24} \rightleftharpoons \text{O}^{\text{H}}_{24}$ reaction, we use the mean open time, $\tau^{\text{H}}_{\text{o}} = 30$ ms, of the channel in the H mode in optimal conditions ($\mathcal{C} = 1\ \mu$M, $\mathcal{I} = 10\ \mu$M). The mean time to transition from O^{H}_{24} to C^{H}_{24} is equal to $K_{O^H_{24}}\mathcal{C}^2\mathcal{I}^4/(j^{HH}_{2424}\mathcal{C}^2\mathcal{I}^2)$. Knowing $K_{O^H_{24}}$, we can calculate j^{HH}_{2424}. Similarly, to estimate the flux parameter j_{2424} for $\text{O}^{\text{H}}_{24} \rightleftharpoons \text{O}^{\text{I}}_{24}$ reaction, we write the mean transition time from O^{H}_{24} to O^{I}_{24} as $K_{O^H_{24}}\mathcal{C}^2\mathcal{I}^4/(j_{2424}\mathcal{C}^2\mathcal{I}^2)$. Knowing the H mode life-time, $\tau^{\text{H}} = 2.7$ sec, in optimal conditions and $K_{O^H_{24}}$, we can estimate j_{2424}.

The flux parameters required for the transition from states with 0 IP_3 bound to states

with 4 IP_3 bound: j_{0001}, j_{0304}, j_{2030}, j_{3132} and j_{3334}, are obtained by fitting the experimental latency distributions for IP_3 and Ca^{2+}/ IP_3 activation. The H mode lifetime at 100 nM and 1 μM Ca^{2+} give us j_{0414} and j_{1424}. j^{HH}_{2424} and j^{II}_{2424} are fixed according to the mean H and I mode open times at optimal ligand concentrations: $\mathcal{C} = 1$ μM and $\mathcal{I} = 10$ μM. We slightly adjust these two parameters so that the model can also give the correct mean open and closed times of the channel. (Superscripts are used on the flux parameters as needed when there were more than one transition between complexes with the same numbers of ligands bound.) We fix j_{0404} according to the L mode lifetime at $\mathcal{C} = 100$ nM and $\mathcal{I} = 10$ μM; and j^{II}_{0414} according to the mean Ca^{2+} activation latency. The mean Ca^{2+} inhibition latency is used to estimate j_{2434}. Finally, the three flux parameters used for the $\mathrm{C}^{\mathrm{I}}_{04} \rightleftharpoons \mathrm{C}^{\mathrm{L}}_{34}$ reaction are fixed so that the following two observations at $\mathcal{I} = 10$ μM were satisfied: (1) 9 out of 103 experiments failed to cause channel bursting when Ca^{2+} was jumped from < 10 nM to 300 μM and (2) 6 out of 94 times the channel has a burst of activity before getting deactivated when Ca^{2+} was dropped from 300 μM to $<$ 10 nM. Although we estimate the initial values of flux parameters from observations, the initial guess proved unnecessary for the fit. The fit converged to the same final parameter values for random initial conditions.

Once we have the initial guess for all the flux parameters in the model, we perform automated fit on the model using all data from ligand jump experiments and time series data at three Ca^{2+} concentrations ($\mathcal{C} = 100$ nM, 1 μM, and 89 μM and fixed $\mathcal{I} = 10$ μM). We choose the best fit according to the AIC and Log-Likelihood scores as described in the main text. The final flux parameters for the model obtained from the fit are given in Table S3.

1.8 Mean Open and Closed Times

In the following, we derive expressions for mean open and closed times. The equilibrium flux from an open state to the closed state is the product of the occupancy of the open state and the sum of transition rates out of the open state. Thus the total equilibrium flux from the 3 open states to the closed states, J, is given as:

$$\begin{aligned} J = K_{\mathrm{O}^{\mathrm{H}}_{24}} \mathcal{C}^2 \mathcal{I}^4 \times (\text{Rate from } \mathrm{O}^{\mathrm{H}}_{24} \text{ to } \mathrm{C}^{\mathrm{H}}_{24} + \text{Rate from } \mathrm{O}^{\mathrm{H}}_{24} \text{ to } \mathrm{C}^{\mathrm{L}}_{34}) \\ + K_{\mathrm{O}^{\mathrm{I}}_{24}} \mathcal{C}^2 \mathcal{I}^4 \times \text{Rate from } \mathrm{O}^{\mathrm{I}}_{24} \text{ to } \mathrm{C}^{\mathrm{I}}_{24} \\ + K_{\mathrm{O}^{\mathrm{I}}_{14}} \mathcal{C} \mathcal{I}^4 \times \text{Rate from } \mathrm{O}^{\mathrm{I}}_{14} \text{ to } \mathrm{C}^{\mathrm{I}}_{04} \end{aligned} \tag{24}$$

The mean open and closed times are given as

$$\tau_o = \frac{P_o(\mathcal{C}, \mathcal{I})}{J} \tag{25}$$

$$\tau_c = \frac{1 - P_o(\mathcal{C}, \mathcal{I})}{J} \tag{26}$$

1.9 Dwell-Time Distributions

In the following, we derive the expressions for the open and closed dwell time distributions. We partition the W matrix into W_C and W_O, where W_C is a diagonal matrix of the equilibrium occupancies of the 9 closed states and W_O is a diagonal matrix of the equilibrium occupancies of the 3 open states in the model. For the modal dwell time distributions, W_C is a diagonal matrix of the equilibrium occupancies of all closed states in a given mode (C^{I}_{04}, C^{I}_{24} for I mode and C^{H}_{24} for H mode) and W_O is a diagonal matrix of the equilibrium occupancies of all open states in the mode (O^{I}_{14}, O^{I}_{24} for I mode and O^{H}_{24} for H mode). Similarly, we can write Q as

$$Q = \begin{pmatrix} Q_{OO} & Q_{OC} \\ Q_{CO} & Q_{CC} \end{pmatrix} \tag{27}$$

Where Q_{OC} is a matrix of the transition rates from all open to all closed states in the model etc. In case of the modal distributions, Q_{OC} is a matrix of the transition rates from all open to all closed states in the I mode or H mode depending on the mode the channel is gating in etc. The open time distribution is the probability density for a channel that opened at time 0 to close for the first time at t_O. The probability that the channel first closed at time t_O is given by

$$\frac{dp_O}{dt} = p_O Q_{OO} \tag{28}$$

which has solution $p_o(t_o) = \pi_O exp(Q_{OO} t_O)$. The probability, F_O, that the channel remains open at time t_O is the sum of the probability over all the open states:

$$F_O(t_O) = \pi_O exp(Q_{OO} t_O) u_O \tag{29}$$

Where u_O and u_C are column vectors of all ones having dimensions equal to the number of open and close states respectively. The probability, G_C, that the channel closes for the first time at time t_O is $G_C(t_O) = 1 - F_O(t_O)$. The open-time distribution, $f_O(t_O)$ is defined by:

$$\int_0^{t_O} f_O(t)dt = G_C(t_O) \tag{30}$$

or $f_O(t_O) = dG_C(t_O)/dt_O$ so that

$$f_O(t_O) = -\pi_O exp(Q_{OO}t_O)Q_{OO}u_O \tag{31}$$

which can be written as

$$f_O(t_O) = \pi_O exp(Q_{OO}t_O)Q_{OC}u_C \tag{32}$$

Similarly, the closed time distribution is given as

$$f_C(t_C) = \pi_C exp(Q_{CC}t_C)Q_{CO}u_O \tag{33}$$

The initial probabilities of open and closed states being occupied at equilibrium are given as

$$\pi_O = \frac{W_C Q_{CO}}{J} \tag{34}$$

$$\pi_C = \frac{W_O Q_{OC}}{J} \tag{35}$$

where $J = W_C Q_{CO} u_O = W_O Q_{OC} u_C$ is the total flux from all open states to all closed states and vice versa. For the modal dwell distributions, J is the total flux from all open states to all closed states in the mode and vice versa.

1.10 Experimental Methods

The experimental data presented is this paper is reproduced from (Ionescu et al., 2006, 2007; Mak et al., 2007). The P_{o} τ_{o} and τ_{c} data is taken from (Ionescu et al., 2006), the modal data is from (Ionescu et al., 2007), and the rapid-perfusion data is adopted from (Mak et al., 2007). Here we present the experimental methods briefly and refer the reader for detailed description to (Ionescu et al., 2006, 2007; Mak et al., 2007).

1.10.1 Measuring P_o, τ_o, and τ_c (Ionescu et al., 2006)

Spodoptera frugiperda (Sf9) cells (Invitrogen) were grown and maintained in SF-900II serum-free media (Gibco) in suspension culture according to the manufacturers protocols. For maximum detection of functional IP_3R channels in patch-clamp experiments, each freshly thawed batch of cells was passaged 3-4 times before being used for electrophysiology. Cells were propagated for up to 7-8 weeks in culture before a new batch was thawed and expanded. Cells were moved from suspension culture to a T-25 flask, allowed to attach to the bottom of the flask for 1 h, and then washed twice with Ca^{2+} - and Mg^{2+} - free PBS. An ice-cold nuclear isolation solution, containing (mM): 140 KCl, 250 sucrose, 1.5 β-mercaptoethanol, 10 Tris-HCl (pH adjusted to 7.4), with complete protease inhibitor cocktail (Roche Molecular Biochemicals, Indianapolis, IN, USA) and 0.05 mM phenylmethylsulphonylfluoride (PMSF), was added to the flask and the cells were detached by gentle scraping. Homogenization of 1-2 ml of the mixture was performed using 2-4 strokes of the pestle in an ice-cold Dounce homogenizer. A 20-30 μl volume of the homogenized mixture was added to 1 ml standard bath solution (mM: 140KCl, 10 Hepes, 0.5 BAPTA, pH 7.3, and free Ca^{2+} adjusted to $\sim$300 nM) in an experimental chamber on the stage of an inverted microscope. Isolated nuclei are $\sim$10 μm in diameter, and were distinguished from intact cells based on their unique morphology. Fresh homogenizations were performed every 2 h. The standard pipette solution contained (mM): 140 KCl, 0.5 Na_2ATP, 10 Hepes, pH 7.3, and various Ca^{2+} and IP_3 concentrations, as indicated. All solutions were carefully buffered to desired free Ca^{2+} (Mak et al., 1998), confirmed by fluorometry.

All experiments were performed at room temperature with the pipette electrode at +20 mV relative to the reference-bath electrode. Each data point shown in P_o, τ_o, and τ_c plots (Fig. 2, Fig. 6A, Fig. 6B, main text) is the mean of results from at least four separate patch-clamp experiments performed under the same conditions. Error bars indicate the SEM. Single channel currents were amplified by an Axopatch-1D amplifier (Axon Instruments, Foster City, CA), filtered at 1 kHz, digitized at 5 kHz (Mak et al., 1998). Segments of current traces exhibiting one or two IP_3R channels were used for open probability P_o determinations (Mak and Foskett, 1997), and single-channel traces were used for dwell-time analyses by QuB software (Qin et al., 2000).

1.10.2 Modal Gating Data (Ionescu et al., 2007)

Nuclear patch clamping was performed as described above (Mak et al., 1998; Ionescu et al., 2006). To maximize the duration of the observed channel activity, current recording was

started as soon as seal resistance exceeded 150MΩ. The standard pipette solution contained (in mM) 140 KCl, 10 HEPES (pH 7.3 by KOH), 0.5 Na_2ATP, 0.5 Ca^{2+} chelator, and various Ca^{2+} and $10\mu M$ IP_3 concentrations as indicated in Fig. 4A-C, main text. The bath solution contained (in mM) 140 KCl, 10 HEPES (pH 7.3 by KOH), 0.5 BAPTA (1,2-bis(*O*-aminophenoxy) ethane-N,N,N,N-tetraacetic acid; Molecular Probes), and 0.225 $CaCl_2$ (free Ca^{2+} concentration = 300 nM). All solutions were carefully buffered to desired free Ca^{2+} concentration using Ca^{2+} chelators with appropriate affinities (Mak et al., 1998), confirmed by fluorometry. All current traces used for analysis were recorded under +20 mV in room temperature. Data were acquired using an Axopatch 200B amplifier (Axon Instruments), filtered at 1 kHz, and digitized at 5 kHz with an ITC-16 interface (Instrutech) and Pulse software (HEKA Electronik).

Segments of current records exhibiting current levels for a single IP_3R channel were idealized using QuB software with SKM (Qin et al., 2000). Channel gating kinetics and modal gating behaviors were characterized using the algorithm in the Appendix of (Ionescu et al., 2007) written using Igor Pro software (WaveMetrics). Statistical analyses were performed on thousands of seconds of single channel current records in Igor Pro software.

1.10.3 Rapid-Perfusion Experiments (Mak et al., 2007)

Single-channel patch-clamp studies of IP_3R channels in a native membrane environment using isolated nuclei from cultured insect Sf9 cells were performed as described above in cyto-out excised patch configuration. The cytoplasmic side of the nuclear membrane patch and of any IP_3R channels therein was exposed to different perfusing solutions containing various ligand concentrations during a continuous patch-clamp recording using a rapid perfusion set-up. Activation latency is the duration between the solution switch time and the first observed channel opening event in response to the solution switch. Similarly, deactivation latency is the duration between solution switch time and the last observed channel closing. The times when the solution was changed at the excised membrane containing the IP_3R channel were clearly marked by an abrupt, discernible change in the baseline current because the alternating solutions containing different $\mathcal{I}$ or $\mathcal{C}$ also contained different concentrations of KCl. The analysis allows latencies >5ms to be clearly and consistently resolved. Current traces from cyto-out membrane patches containing one to several (≤ 10) active IP_3R channels were selected for latency analysis. All current records were acquired with + 20 mV applied potential at room temperature.

The latency distributions shown in Fig. 5 (and Fig. 8) of the main text are based on

the n number of solution switches and N number of cyto-out patches, where (n, N) for Fig. 5A-H (and Fig. 8A-H) respectively are: (458,14), (260,14), (532,11), (376,11), (638,7), (458,7), (186,7), and (197,7). The (n,N) values for the experiments involving $(\mathcal{C}, \mathcal{I})$ changes from $(0\mu\text{M}, 10\mu\text{M})$ to $(300\mu\text{M}, 10\mu\text{M})$ and from $(300\mu\text{M}, 10\mu\text{M})$ to $(0\mu\text{M}, 10\mu\text{M})$ were (94,3) and (70,3) respectively.

References

Bruno, W. J., J. Yang, and J. E. Pearson. 2005. Using independent open-to-closed transitions to simplify aggregated Markov models of ion channel gating kinetics. *Proc. Natl. Acad. Sci. USA*. 102:6326–6331.

Ionescu, L., K. H. Cheung, H. Vais, D. O. D. Mak, C. White, and J. K. Foskett. 2006. Graded recruitment and inactivation of single IP_3R Ca^{2+}-release channels: implications for quartal Ca^{2+} release. *J. Physiol.* 573:645–662.

Ionescu, L., C. White, K. H. Cheung, J. Shuai, I. Parker, J. E. Pearson, J. K. Foskett, and D. O. D. Mak. 2007. Mode switching is the major mechanism of ligand regulation of IP_3R Ca^{2+} release channels. *J. Gen. Physiol.* 130:631–645.

Mak, D. O. D., and J. K. Foskett. 1997. Single-channel kinetics, inactivation, and spatial distribution of inositol trisphosphate (IP_3R) receptors in Xenopus oocyte nucleus. *J. Gen. Physiol.* 109:571.

Mak, D. O. D., S. McBride, and J. K. Foskett. 1998. IP_3 activation of IP_3R Ca^{2+} channel by ligand tuning of Ca^{2+} inhibition. *Proc. Natl. Acad. Sci. USA*. 95:15821–15825.

Mak, D. O. D., J. E. Pearson, K. P. C. Loong, S. Datta, M. Fernandez-Mongil, and J. K. Foskett. 2007. Rapid ligand-regulated gating kinetics of single IP_3R Ca^{2+} release channels. *EMBO Reports*. 8:1044–1051.

Qin, F., A. Auerbach, and F. Sachs. 2000. A direct optimization approach to hidden markov modeling for single channel kinetics. *Biophys J.* 79:1915–1927.

Snedecor, G., and W. Cochran. 1989. Statistical Methods. Iowa State University Press, Ames, IA.

Song, L., and K. Magleby. 1994. Testing for microscopic reversibility in the gating of maxi k+ channels using two-dimensional dwell-time distributions. *Biophys. J.* 67:91–104.

Yang, J., W. J. Bruno, W. S. Hlavacek, and J. E. Pearson. 2006. On imposing detailed balance in complex reaction mechanisms. *Biophys. J.* 91:1136–1141.

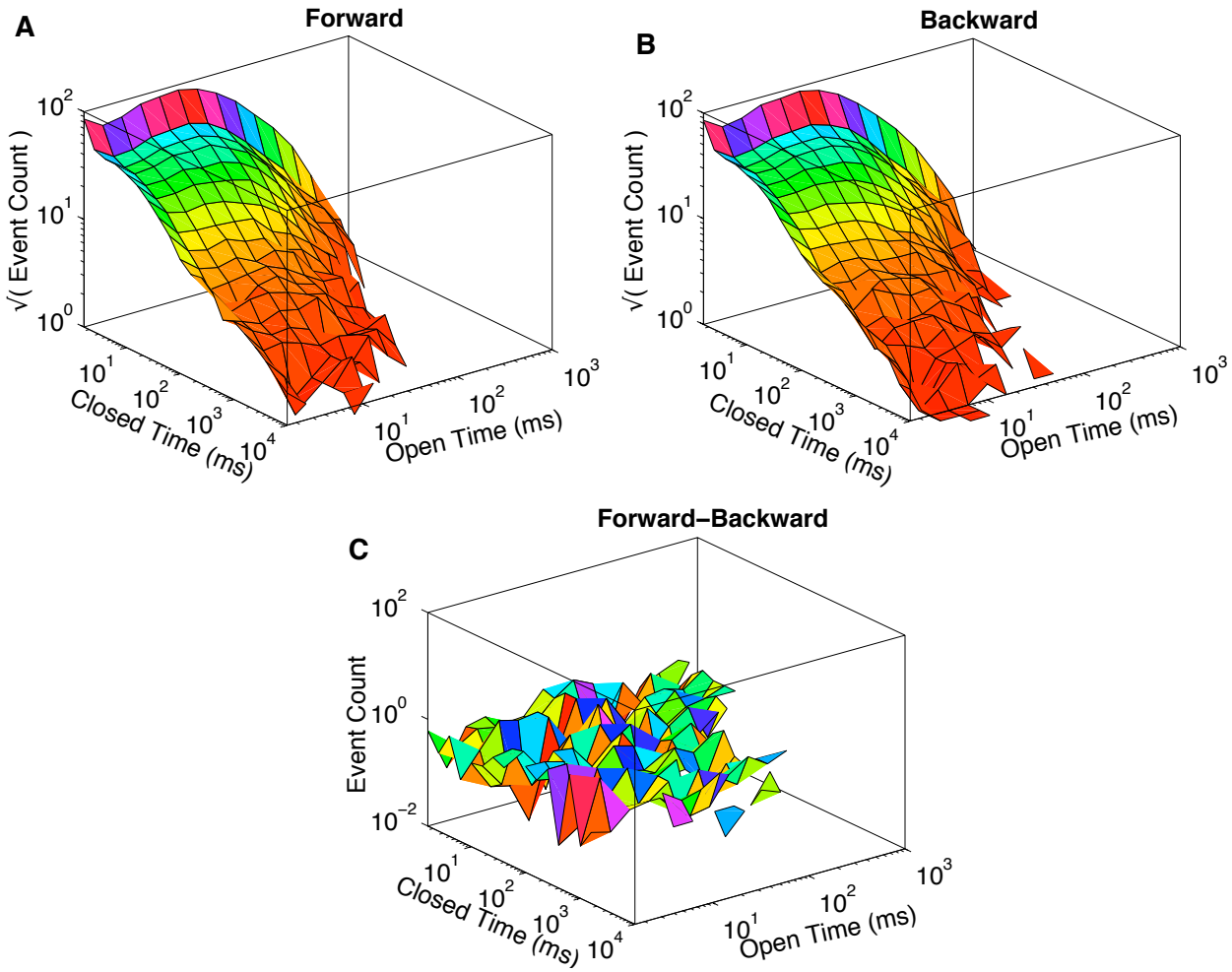

Fig. S1: Two-dimensional dwell-time distributions for open-closed intervals of IP_3R. (A) Two-dimensional distribution obtained from forward and (B) backward analysis of the time-series data. The z-axis is the square-root of the number of events in a given bin. (C) Difference between forward and backward distributions.

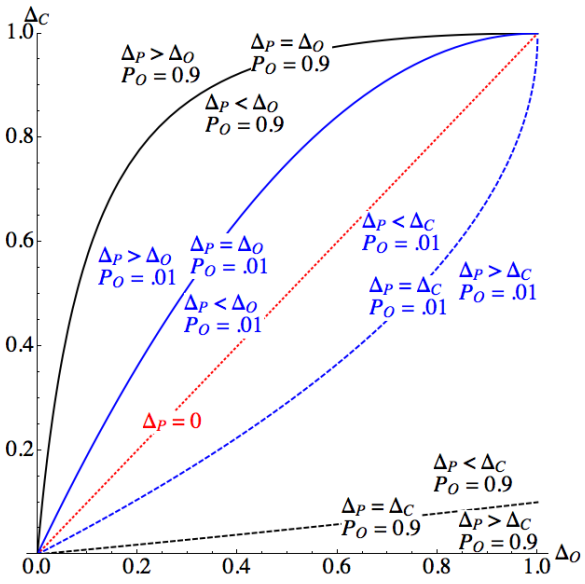

Fig. S2: Error in P_{o} verses error in $\tau_{\mathrm{o}}$and τ_{c}. Various lines and regions shown here are described in the text.

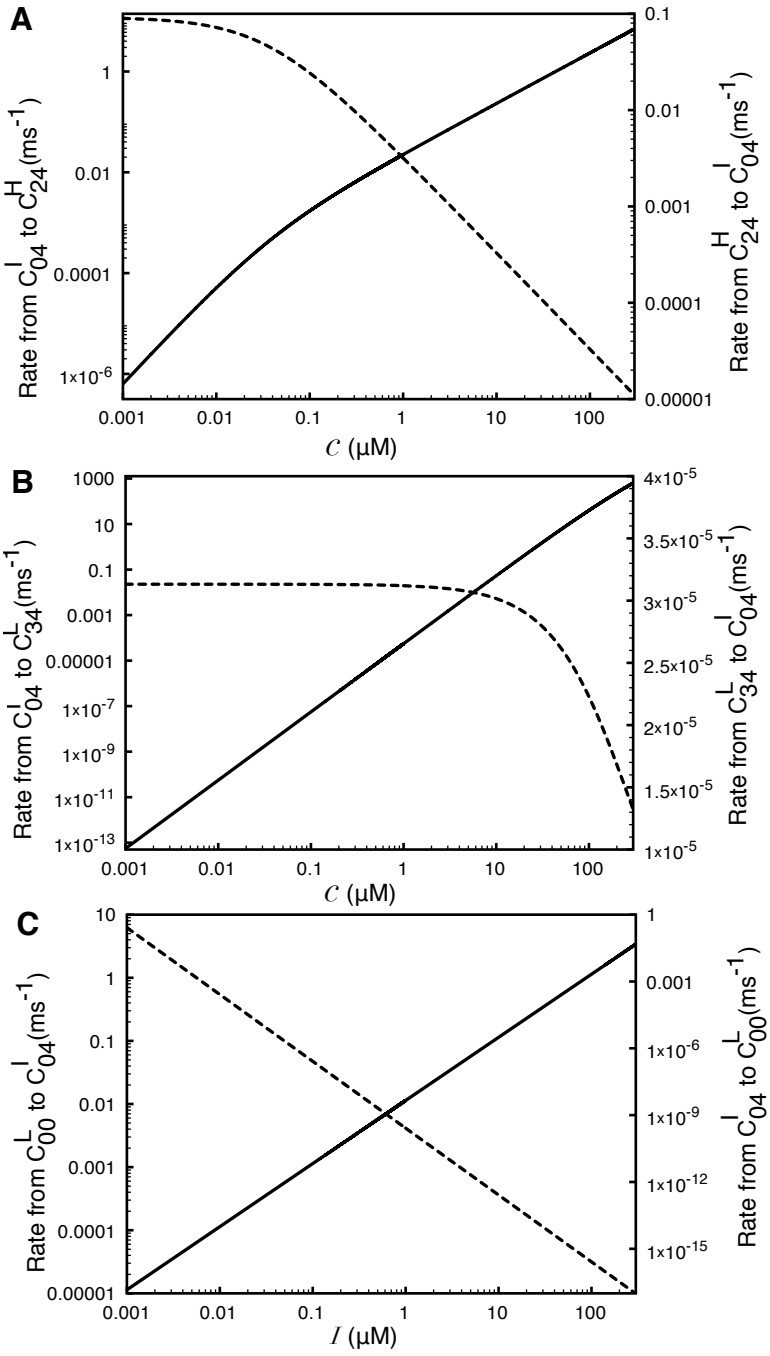

Fig. S3: Ligand dependence of transition rates for the model. Transition rates that are not shown here are either constants or linearly increasing functions of $\mathcal{C}$ or $\mathcal{I}$. Solid and dashed curves correspond to vertical axes on left and right, respectively. $\mathcal{I} = 10$ μM for (A and B) and $\mathcal{C} = 2$ μM for (C).

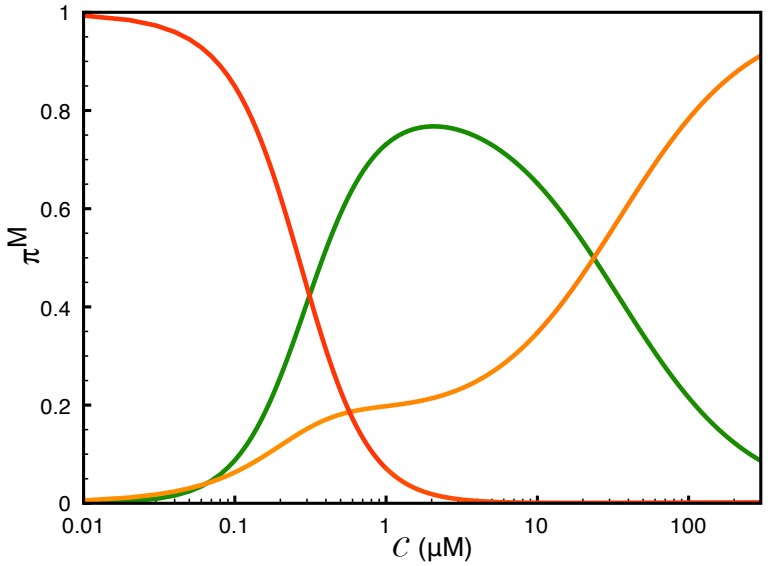

Fig. S4: Relative prevalence, π^{M}, as a function of $\mathcal{C}$ for the three modes when $\mathrm{C}_{34}^{\mathrm{L}}$ state is included in the I mode instead of $\mathrm{C}_{04}^{\mathrm{I}}$. Red, orange, and green curves represent L, I, and H modes respectively.

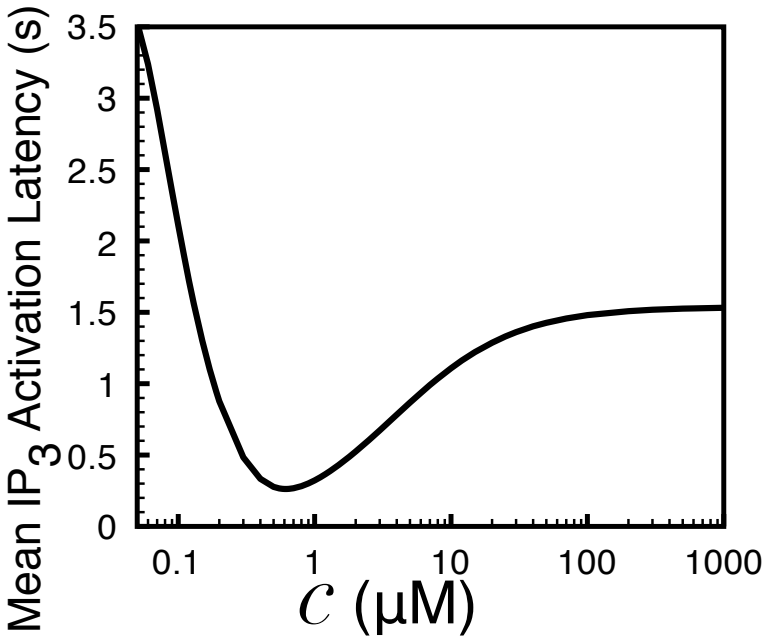

Fig. S5: Model derived mean IP_3 activation latency as a function of $\mathcal{C}$.

Table S1: **Parameters for occupancies of all states in the CM model.**

Parameters	Values
$K_{\mathrm{C}_{00}^{\mathrm{L}}}$	1
$K_{\mathrm{C}_{32}^{\mathrm{L}}}$	$1.479 \times 10^{7}\ \mu\mathrm{M}^{-5}$
$K_{\mathrm{C}_{34}^{\mathrm{L}}}$	$7.762 \times 10^{7}\ \mu\mathrm{M}^{-7}$
$K_{\mathrm{O}_{14}^{\mathrm{I}}}$	$1.202 \times 10^{8}\ \mu\mathrm{M}^{-5}$
$K_{\mathrm{C}_{04}} = K_{\mathrm{C}_{04}^{\mathrm{L}}} + K_{\mathrm{C}_{04}^{\mathrm{I}}}$	$2.183 \times 10^{8}\ \mu\mathrm{M}^{-4}$
$K_{\mathrm{C}_{24}} = K_{\mathrm{C}_{24}^{\mathrm{H}}} + K_{\mathrm{C}_{24}^{\mathrm{I}}}$	$6.165 \times 10^{8}\ \mu\mathrm{M}^{-6}$
$K_{\mathrm{O}_{24}} = K_{\mathrm{O}_{24}^{\mathrm{H}}} + K_{\mathrm{O}_{24}^{\mathrm{I}}}$	$2.042 \times 10^{9}\ \mu\mathrm{M}^{-6}$
p	0.8
r	0.95
$K_{\mathrm{C}_{04}^{\mathrm{L}}}$	$pK_{\mathrm{C}_{04}}$
$K_{\mathrm{C}_{04}^{\mathrm{I}}}$	$(1-p)K_{\mathrm{C}_{04}}$
$K_{\mathrm{O}_{24}^{\mathrm{H}}}$	$rK_{\mathrm{O}_{24}}$
$K_{\mathrm{O}_{24}^{\mathrm{I}}}$	$(1-r)K_{\mathrm{O}_{24}}$
$K_{\mathrm{C}_{24}^{\mathrm{H}}}$	$0.5K_{\mathrm{C}_{24}}$
$K_{\mathrm{C}_{24}^{\mathrm{I}}}$	$(1-0.5)K_{\mathrm{C}_{24}}$
$K_{\mathrm{C}_{20}^{\mathrm{L}}}$	$2.5\ \mu\mathrm{M}^{-2}$
$K_{\mathrm{C}_{30}^{\mathrm{L}}}$	$0.15\ \mu\mathrm{M}^{-3}$

Table S2: **Transition rates between various states in the CM model.**

Transition	Rates
$\mathrm{C}^{\mathrm{I}}_{04} \rightarrow \mathrm{C}^{\mathrm{H}}_{24}$	$rsr(j_{0414}\mathcal{C},\ j_{1424}\mathcal{C}^2)/K_{\mathrm{C}^{\mathrm{I}}_{04}}$
$\mathrm{C}^{\mathrm{I}}_{04} \leftarrow \mathrm{C}^{\mathrm{H}}_{24}$	$rsr(j_{0414}\mathcal{C},\ j_{1424}\mathcal{C}^2)/K_{\mathrm{C}^{\mathrm{H}}_{24}}\mathcal{C}^2$
$\mathrm{C}^{\mathrm{H}}_{24} \rightarrow \mathrm{O}^{\mathrm{H}}_{24}$	$j^{\mathrm{HH}}_{2424}/K_{\mathrm{C}^{\mathrm{H}}_{24}}$
$\mathrm{C}^{\mathrm{H}}_{24} \leftarrow \mathrm{O}^{\mathrm{H}}_{24}$	$j^{\mathrm{HH}}_{2424}/K_{\mathrm{O}^{\mathrm{H}}_{24}}$
$\mathrm{O}^{\mathrm{H}}_{24} \rightarrow \mathrm{C}^{\mathrm{L}}_{34}$	$j_{2434}\mathcal{C}/K_{\mathrm{O}^{\mathrm{H}}_{24}}$
$\mathrm{O}^{\mathrm{H}}_{24} \leftarrow \mathrm{C}^{\mathrm{L}}_{34}$	$j_{2434}/K_{\mathrm{C}^{\mathrm{L}}_{34}}$
$\mathrm{C}^{\mathrm{I}}_{04} \rightarrow \mathrm{C}^{\mathrm{L}}_{34}$	$rsr(j^{\mathrm{IL}}_{0414}\mathcal{C},\ j^{\mathrm{IL}}_{1424}\mathcal{C}^2,\ j^{\mathrm{IL}}_{2434}\mathcal{C}^3)/K_{\mathrm{C}^{\mathrm{I}}_{04}}$
$\mathrm{C}^{\mathrm{I}}_{04} \leftarrow \mathrm{C}^{\mathrm{L}}_{34}$	$rsr(j^{\mathrm{IL}}_{0414}\mathcal{C},\ j^{\mathrm{IL}}_{1424}\mathcal{C}^2,\ j^{\mathrm{IL}}_{2434}\mathcal{C}^3)/K_{\mathrm{C}^{\mathrm{L}}_{34}}\mathcal{C}^3$
$\mathrm{C}^{\mathrm{I}}_{04} \rightarrow \mathrm{O}^{\mathrm{I}}_{14}$	$j^{\mathrm{II}}_{0414}\mathcal{C}/K_{\mathrm{C}^{\mathrm{I}}_{04}}$
$\mathrm{C}^{\mathrm{I}}_{04} \leftarrow \mathrm{O}^{\mathrm{I}}_{14}$	$j^{\mathrm{II}}_{0414}/K_{\mathrm{O}^{\mathrm{I}}_{14}}$
$\mathrm{C}^{\mathrm{I}}_{24} \rightarrow \mathrm{O}^{\mathrm{I}}_{24}$	$j^{\mathrm{II}}_{2424}/K_{\mathrm{C}^{\mathrm{I}}_{24}}$
$\mathrm{C}^{\mathrm{I}}_{24} \leftarrow \mathrm{O}^{\mathrm{I}}_{24}$	$j^{\mathrm{II}}_{2424}/K_{\mathrm{O}^{\mathrm{I}}_{24}}$
$\mathrm{O}^{\mathrm{I}}_{24} \rightarrow \mathrm{O}^{\mathrm{H}}_{24}$	$j_{2424}/K_{\mathrm{O}^{\mathrm{I}}_{24}}$
$\mathrm{O}^{\mathrm{I}}_{24} \leftarrow \mathrm{O}^{\mathrm{H}}_{24}$	$j_{2424}/K_{\mathrm{O}^{\mathrm{H}}_{24}}$
$\mathrm{C}^{\mathrm{I}}_{04} \rightarrow \mathrm{C}^{\mathrm{L}}_{04}$	$j_{0404}/K_{\mathrm{C}^{\mathrm{I}}_{04}}$
$\mathrm{C}^{\mathrm{I}}_{04} \leftarrow \mathrm{C}^{\mathrm{L}}_{04}$	$j_{0404}/K_{\mathrm{C}^{\mathrm{L}}_{04}}$
$\mathrm{C}^{\mathrm{L}}_{32} \rightarrow \mathrm{C}^{\mathrm{L}}_{34}$	$j_{3334}\mathcal{I}^2/K_{\mathrm{C}^{\mathrm{L}}_{32}}$
$\mathrm{C}^{\mathrm{L}}_{32} \leftarrow \mathrm{C}^{\mathrm{L}}_{34}$	$j_{3334}/K_{\mathrm{C}^{\mathrm{L}}_{34}}$
$\mathrm{C}^{\mathrm{L}}_{30} \rightarrow \mathrm{C}^{\mathrm{L}}_{32}$	$j_{3132}\mathcal{I}^2/K_{\mathrm{C}^{\mathrm{L}}_{30}}$
$\mathrm{C}^{\mathrm{L}}_{30} \leftarrow \mathrm{C}^{\mathrm{L}}_{32}$	$j_{3132}/K_{\mathrm{C}^{\mathrm{L}}_{32}}$
$\mathrm{C}^{\mathrm{L}}_{20} \rightarrow \mathrm{C}^{\mathrm{L}}_{30}$	$j_{2030}\mathcal{C}/K_{\mathrm{C}^{\mathrm{L}}_{20}}$
$\mathrm{C}^{\mathrm{L}}_{20} \leftarrow \mathrm{C}^{\mathrm{L}}_{30}$	$j_{2030}/K_{\mathrm{C}^{\mathrm{L}}_{30}}$
$\mathrm{C}^{\mathrm{L}}_{00} \rightarrow \mathrm{C}^{\mathrm{I}}_{04}$	$rsr(j_{0001}\mathcal{I},\ j_{0304}\mathcal{I}^4)$
$\mathrm{C}^{\mathrm{L}}_{00} \leftarrow \mathrm{C}^{\mathrm{I}}_{04}$	$rsr(j_{0001},\ j_{0304}\mathcal{I}^3)/K_{\mathrm{C}^{\mathrm{I}}_{04}}\mathcal{I}^3$
$\mathrm{C}^{\mathrm{L}}_{20} \rightarrow \mathrm{C}^{\mathrm{H}}_{24}$	$rsr(j_{2021}\mathcal{I},\ j_{2324}\mathcal{I}^4)$
$\mathrm{C}^{\mathrm{L}}_{20} \leftarrow \mathrm{C}^{\mathrm{H}}_{24}$	$rsr(j_{2021},\ j_{2324}\mathcal{I}^3)/K_{\mathrm{C}^{\mathrm{I}}_{04}}\mathcal{I}^3$

Table S3: **Flux parameters used in the CM model.** Superscripts are used to distinguish between different flux parameters that connect different pairs of states that have the same numbers of ligands bound. For example, in both transitions $C^{I}_{24} \rightleftharpoons O^{I}_{24}$ and $C^{H}_{24} \rightleftharpoons O^{H}_{24}$, C^{I}_{24} and C^{H}_{24} are bound to the same number of Ca^{2+} and IP_3, and so are O^{I}_{24} and O^{H}_{24}. However, the two transitions have different flux parameters. TS stands for time-series data.

Parameters	Pathway	Values from Latency+TS fit	Values from Latency fit	Units
j_{0414}	$C^{I}_{04} \rightleftharpoons C^{H}_{24}$	1.017×10^{6}	4.213×10^{-3}	$\mu M^{-5} ms^{-1}$
j_{1424}	$C^{I}_{04} \rightleftharpoons C^{H}_{24}$	2.840×10^{7}	8.882×10^{5}	$\mu M^{-6} ms^{-1}$
j_{2434}	$O^{H}_{24} \rightleftharpoons C^{L}_{34}$	4.663×10^{4}	2.733×10^{7}	$\mu M^{-7} ms^{-1}$
j^{IL}_{0414}	$C^{I}_{04} \rightleftharpoons C^{L}_{34}$	9.502×10^{8}	4.981×10^{4}	$\mu M^{-5} ms^{-1}$
j^{IL}_{1424}	$C^{I}_{04} \rightleftharpoons C^{L}_{34}$	6.4×10^{5}	4.730×10^{3}	$\mu M^{-6} ms^{-1}$
j^{IL}_{2434}	$C^{I}_{04} \rightleftharpoons C^{L}_{34}$	2.431×10^{3}	9.438×10^{3}	$\mu M^{-7} ms^{-1}$
j_{2030}	$C^{L}_{20} \rightleftharpoons C^{L}_{30}$	2.449×10^{-3}	3.1732×10^{7}	$\mu M^{-3} ms^{-1}$
j^{II}_{0414}	$C^{I}_{04} \rightleftharpoons O^{I}_{14}$	4.966×10^{4}	1.573×10^{-2}	$\mu M^{-5} ms^{-1}$
j^{II}_{2424}	$C^{I}_{24} \rightleftharpoons O^{I}_{24}$	1.467×10^{7}	4.214×10^{8}	$\mu M^{-7} ms^{-1}$
j_{2424}	$O^{I}_{24} \rightleftharpoons O^{H}_{24}$	3.301×10^{5}	1.050×10^{-3}	$\mu M^{-6} ms^{-1}$
j_{0404}	$C^{I}_{04} \rightleftharpoons C^{L}_{04}$	5.459×10^{4}	1.288×10^{7}	$\mu M^{-4} ms^{-1}$
j^{HH}_{2424}	$C^{H}_{24} \rightleftharpoons O^{H}_{24}$	7.723×10^{7}	1.417×10^{5}	$\mu M^{-6} ms^{-1}$
j_{3132}	$C^{L}_{30} \rightleftharpoons C^{L}_{34}$	2.891×10^{-2}	6.648×10^{6}	$\mu M^{-5} ms^{-1}$
j_{3334}	$C^{L}_{32} \rightleftharpoons C^{L}_{34}$	2.120×10^{3}	3.425×10^{5}	$\mu M^{-7} ms^{-1}$
j_{0001}	$C^{L}_{00} \rightleftharpoons C^{I}_{04}$	1.138×10^{-2}	7.003×10^{3}	$\mu M^{-1} ms^{-1}$
j_{0304}	$C^{L}_{00} \rightleftharpoons C^{I}_{04}$	4.756×10^{10}	5.305×10^{7}	$\mu M^{-4} ms^{-1}$
j_{2021}	$C^{L}_{20} \rightleftharpoons C^{H}_{24}$	8.904×10^{-4}	8.843×10^{-2}	$\mu M^{-3} ms^{-1}$
j_{2324}	$C^{L}_{20} \rightleftharpoons C^{H}_{24}$	8.523×10^{6}	3.003×10^{3}	$\mu M^{-6} ms^{-1}$

Table S4: **Occupancy parameters for De Young-Keizer model**

Parameters	Values
K_{000}	1
K_{001}	3.724×10^2 μM^{-1}
K_{010}	1.208×10^4 μM^{-1}
K_{011}	4.077×10^3 μM^{-2}
K_{100}	3.786×10^4 μM^{-1}
K_{101}	1.242×10^4 μM^{-2}
K_{110}	4.525×10^5 μM^{-2}
K_{111}	5.621×10^3 μM^{-3}

Table S5: **Rate constants for De Young-Keizer model. TS stands for time-series data.**

Parameters	Values from Latency+TS fit	Values from Latency fit	Units
$k_{000\to100}$	6.011×10^{-4}	7.716×10^{-3}	$\mathrm{ms}^{-1}\mu\mathrm{M}^{-1}$
$k_{000\leftarrow100}$	1.588×10^{-8}	2.038×10^{-7}	ms^{-1}
$k_{010\to110}$	5.213×10^{-1}	8.408×10^{-3}	$\mathrm{ms}^{-1}\mu\mathrm{M}^{-1}$
$k_{010\leftarrow110}$	1.388×10^{-2}	2.238×10^{-4}	ms^{-1}
$k_{100\to101}$	9.873×10^{-5}	1.518×10^{-3}	$\mathrm{ms}^{-1}\mu\mathrm{M}^{-1}$
$k_{100\leftarrow101}$	3.010×10^{-4}	4.628×10^{-2}	ms^{-1}
$k_{110\to111}$	3.134×10^{-7}	2.599×10^{-19}	$\mathrm{ms}^{-1}\mu\mathrm{M}^{-1}$
$k_{110\leftarrow111}$	2.523×10^{-5}	2.092×10^{-17}	ms^{-1}
$k_{001\to101}$	1.677×10^{-3}	1.709×10^{-11}	$\mathrm{ms}^{-1}\mu\mathrm{M}^{-1}$
$k_{001\leftarrow101}$	5.031×10^{-5}	5.127×10^{-13}	ms^{-1}
$k_{011\to111}$	2.854×10^{-3}	2.019×10^{-4}	$\mathrm{ms}^{-1}\mu\mathrm{M}^{-1}$
$k_{011\leftarrow111}$	2.070×10^{-3}	1.464×10^{-4}	ms^{-1}
$k_{000\to001}$	1.023×10^{4}	1.525×10^{-9}	$\mathrm{ms}^{-1}\mu\mathrm{M}^{-1}$
$k_{000\leftarrow001}$	27.446	4.094×10^{-12}	ms^{-1}
$k_{010\to011}$	3.05×10^{-3}	3.628×10^{-3}	$\mathrm{ms}^{-1}\mu\mathrm{M}^{-1}$
$k_{010\leftarrow011}$	9.013×10^{-3}	1.072×10^{-2}	ms^{-1}
$k_{000\to010}$	5.190×10^{2}	1.044×10^{-7}	$\mathrm{ms}^{-1}\mu\mathrm{M}^{-1}$
$k_{000\leftarrow010}$	4.308×10^{-2}	8.666×10^{-12}	ms^{-1}
$k_{101\to111}$	4.475×10^{-7}	2.380×10^{-4}	$\mathrm{ms}^{-1}\mu\mathrm{M}^{-1}$
$k_{101\leftarrow111}$	9.887×10^{-7}	5.257×10^{-4}	ms^{-1}
$k_{100\to110}$	3.708×10^{-2}	4.342×10^{-2}	$\mathrm{ms}^{-1}\mu\mathrm{M}^{-1}$
$k_{100\leftarrow110}$	3.102×10^{-3}	3.632×10^{-4}	ms^{-1}
$k_{001\to011}$	2.429×10^{10}	5.083×10^{-3}	$\mathrm{ms}^{-1}\mu\mathrm{M}^{-1}$
$k_{001\leftarrow011}$	2.220×10^{9}	4.646×10^{-4}	ms^{-1}